RESEARCH ARTICLE | JANUARY 15 2019

Upgrade of bending magnet MX beamline BL38B1 at SPring-8

Seiki Baba; Nobuhiro Mizuno; Hideo Okumura; Nipawan Nuemket; Kazuya Hasegawa; Yuki Nakamura; Hironori Murakami; Go Ueno; Tomoki Fukui; Takaki Irie; Masayuki Tanaka; Hiroshi Yamazaki; Haruhiko Ohashi; Masaki Yamamoto; Takashi Kumasaka

AIP Conf. Proc. 2054, 060008 (2019)
https://doi.org/10.1063/1.5084639

Upgrade of bending magnet MX beamline BL38B1 at SPring-8

Seiki Baba[1], Nobuhiro Mizuno[1], Hideo Okumura[1], Nipawan Nuemket[1], Kazuya Hasegawa[1],Yuki Nakamura[1], Hironori Murakami[1], Go Ueno[2], Tomoki Fukui[1], Takaki Irie[1], Masayuki Tanaka[1], Hiroshi Yamazaki[1], Haruhiko Ohashi[1], Masaki Yamamoto[2] and Takashi Kumasaka[1,a)]

[1] *JASRI, 1-1-1, Kouto, Sayo-cho, Sayo-gun, Hyogo 679-5198, JAPAN*
[2] *RIKEN SPring-8 Center, 1-1-1, Kouto, Sayo-cho, Sayo-gun, Hyogo 679-5148, JAPAN*

[a)]Corresponding author: kumasaka@spring8.or.jp

Abstract. The bending magnet beamline BL38B1 at SPring-8 is equipped with X-ray optics consisting of the SPring-8 standard double crystal monochromator (DCM) with Si (111) and a vertically bent cylindrical mirror, which produce available energy ranging from 6 to 17 keV and photon flux of 8.6×10^{10} Ph/sec at 12.4 keV. These moderate beam properties are suited to high throughput cryogenic macromolecular crystallography (MX) using moderately sized crystals (over 100 μm) and non-cryo-cooled MX methodology that takes advantage of the lower X-ray dose rate. However, along with the recent research trends the target crystal sizes have tended to become smaller and smaller, and are currently less than 100 μm. To resolve this issue, we achieved an upgrade of beamline optics for higher flux and higher density X-rays and development of apparatuses for precise diffraction data collection.

INTRODUCTION

The optics design of BL38B1 is based on the standard SPring-8 bending magnet beamline (Figure 1(a)) [1]. X-rays from the source point are truncated with the water-cooled slit at 27.5 m from the light source. This aperture size is set at 8 mm (H) × 1.5 mm (V) to introduce the X-rays to the SPring-8 standard DCM with Si (111) installed at 30 m from the source point [2]. The 1st and 2nd Si (111) crystals in the DCM are cooled by an indirect water-cooling system. To focus the X-ray beam, a vertically bent cylindrical mirror is installed. The X-ray beam properties at the sample position are as follows: energy range from 6 to 17 keV, energy resolution $\Delta E/E$ on the order of 2×10^{-4}, beam size of 100 μm × 200 μm (FWHM H × V), and photon flux of 8.6×10^{10} Ph/sec at 12.4 keV (Figure 2(a)).

MX research is one of the major applications of synchrotrons, and many beamlines are exclusively dedicated to this purpose. Among the SPring-8 MX beamlines, the BL38B1 beamline utilizes moderate beam properties and targets high throughput data collection of cryo-cooled protein crystals by using an automatic sample changer and software [3, 4]. Moreover, we have focused our attention on the lower dose rate and have been developing the methodology for non-cryo-cooled protein crystals by a humidity controlled environment using the HAG method [5]. Recently the target sample size for the protein crystallography has tended to become smaller and smaller. In order to cope with this situation, we have upgraded the beamline optics to utilize higher flux and higher density X-rays and developed κ and φ axes on the goniometer.

UPGRADED BEAMLINE OPTICS

For high-efficiency data collection, improvements in photon flux are an effective way to reduce X-ray irradiation time. In order to generate higher intensity monochromatic X-rays using reduction of energy resolution, the standard

Proceedings of the 13th International Conference on Synchrotron Radiation Instrumentation – SRI2018
AIP Conf. Proc. 2054, 060008-1–060008-4; https://doi.org/10.1063/1.5084639
Published by AIP Publishing. 978-0-7354-1782-3/$30.00

symmetric Si (111) 1st and 2nd crystals were replaced with asymmetrically cut Si (111) 1st and 2nd crystals (Figure 1(a, b)) [6]. The angle of asymmetry of the Si (111) 1st and 2nd crystals was chosen as 6.33° in order to make an energy range of 6 to 15 keV available (Figure 1(b)). By adopting this design, the energy resolution ΔE/E decreases to 1/3 of the original value, but remains on the order of 10^{-4}. At the same time, DCM was improved to stabilize the vibration of the cooling-water pump. As a result, the photon flux increased to 2.22×10^{11} Ph/sec at 13.8 keV, which was 2.6 times the previous flux (Figure 2(a)). Although the advantages of the asymmetric cut decreased at the lower energy range, the photon flux increased by up to 1.6 times even at 6.6 keV.

To reduce scattering noise from the sample, beam shaping is required to adjust the beam size to the crystal size. We developed a beam-defining aperture-insert system by using a tantalum plate pierced with pinholes of various sizes (Φ 20, 30, 50, 100, 150, 200 and 300 μm) for adjusting the beam to crystal sizes of Φ 20 μm to 100 μm × 200 μm (FWHM H × V) (Figure 2 (b)) [7]. This beam-defining system also featured a scattering-guard pinhole (Φ 400 μm) that was inserted between the Ta plate and the sample (Figure 2(c)).When visualizing the sample using an X-ray co-axial CCD camera, the Ta plate and another scattering-guard pinhole are evacuated from the beam axis (Figure 2(c)).

In order to increase the flux density of X-rays, a capillary lens with a focal distance of 50 mm (J12432-01; Hamamatsu Photonics Co.) was implemented as the second focusing optic (Figure 1(a, c)). This capillary-focusing system included a Ta plate pierced with a 300 mm pinhole as a 1st scattering-guard and a scattering-guard pinhole as a 2nd scattering-guard between the capillary lens and the sample, and increased the photon flux to 1.26×10^{11} Ph/sec at 12.4 keV with a beam size of 80 μm diameter at the sample position (Figure 2(c)). The capillary lens and X-ray co-axial camera were switched by vertical movement of the Z axis (Figure 1(c 4)). These systems can be switched automatically at any time as desired by the user (Figure 1(c)).

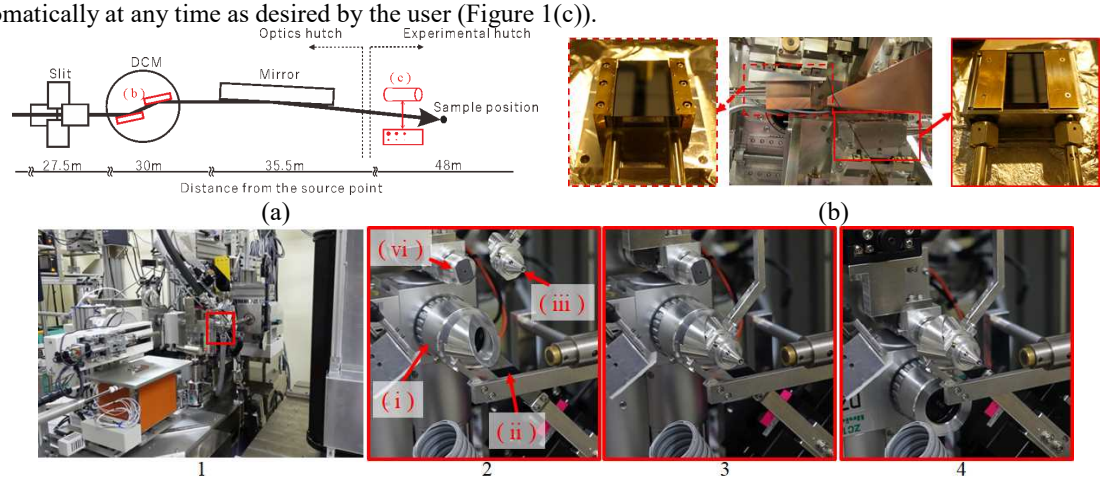

FIGURE 1. Beamline upgrade. (a) Overview of the beamline optics. Distances from the source point and upgraded components (red) are indicated. (b) Crystals and their folders for asymmetric Si (111) 1st (red line box) and 2nd (red dotted line box) crystals installed in DCM at the optics hutch. (c) Overview of the beam-defining system and the capillary-focusing system (red line box) in the experimental hutch: 1, Diffractometer; 2-4, sample mounting environment in the sample-alignment mode (2), beam-defining mode (3), and capillary-focusing mode (4). The switching system was assembled with the following: i, X-ray co-axial camera; ii, Ta pinholes plate; iii, scattering-guard Ta pinhole; and iv, capillary lens.

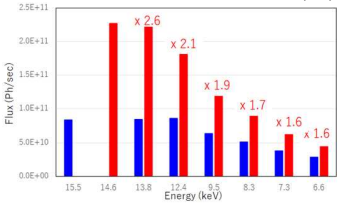

(a)

X-ray optics	Defining φ20 μm	Defining φ30 μm	Defining φ50 μm	Defining φ100 μm	Defining φ150 μm	Defining φ200 μm	Defining φ300 μm	Capillary Focusing
Flux (Ph/sec)	2.89×10^{9}	6.48×10^{9}	1.70×10^{10}	5.57×10^{10}	9.97×10^{10}	1.39×10^{11}	1.85×10^{11}	1.26×10^{11}
Beam profile								

(b)

FIGURE 2. Results of upgrade. (a) Comparison of the photon flux of symmetric (blue) and asymmetric (red) cut crystals in DCM. (b) Flux and beam profiles using the beam-defining system and the capillary-focusing system.

Diffraction experiments were performed using hen egg-white lysozyme of space group $P4_32_12$ (lysozyme ($P4_32_12$)) crystals to evaluate two types of X-ray optics. Datasets were measured in the order of the beam-defining system with the Φ 100 μm pinhole and the capillary-focusing system from the same crystal at a wavelength of 1.5 Å (Table 1). The flux in the latter setting was 5.80×10^{10} Ph/sec, which is twice that of the beam-defining system with a Φ 100 μm beam of 3.23×10^{10} Ph/sec. Thus, the total exposure time in the capillary-focusing system was successfully shortened to half that of the beam-defining system with a Φ 100 μm pinhole (Table 1). The beam divergences of the original mirror focusing and the capillary focusing were simply evaluated by measuring the beam size at two positions, the sample position and 500 mm downstream from sample position, using a beam monitor. The beam divergence was enlarged from 460 μrad × 80 μrad (H × V) to 1.2 mrad × 1.9 mrad (H × V) by the capillary focusing. This approach gives broader diffraction spots [8] and may induce spot overlap from the crystals of large unit cells.

TABLE 1. Experimental conditions and diffraction data statistics. All X-ray diffraction data were collected using a PILATUS3 6M detector at 100 K, and were processed and scaled using XDS [9]. *The maximum resolution of lysozyme ($P4_32_12$) was determined by based on that the completeness of the outer shell of 2nd data was 99.0%. The maximum resolution of lysozyme ($P1$) was determined by based on that the completeness of the outer shell of merged data of 1st, 2nd and 3rd was 99.0%. †Values in parentheses are for the inner and outer resolution shell. ‡Lysozyme ($P4_32_12$) crystal: The crystals were grown using hanging-drop vapour diffusion at 293 K. HEW-lysozyme powder was dissolved in 50 mM sodium acetate buffer pH 4.5 until the concentration was approximately 35 mg/ml. The crystallization drop was set up on an 18 mm coverslip by mixing 5 μl of the protein solution and an equal volume of a solution consisting of 1.6 M sodium chloride and 50 mM sodium acetate buffer pH 4.5. The volume of the reservoir solution, which consisted of 1.0 M sodium chloride and 50 mM sodium acetate buffer pH 4.5, was 500 μl per well. The crystal was flash-cooled by using the HAG method [5]. The coated glue used 10% (w/v) PVA4500 including 5% (v/v) ethylene glycol. The optimized humidity before flash-cooling was 85% R.H. § Lysozyme ($P1$) crystal: The crystals were grown using hanging-drop vapour diffusion at 293 K. HEW-lysozyme powder was dissolved in 50 mM sodium acetate pH 4.5 until the concentration was approximately 25-50 mg/ml. The crystallization drop was set up on an 18 mm coverslip by mixing 2 μl, 2 μl and 0.3 μl of the protein solution, reservoir solution and P1 seeding solution, respectively. The volume of reservoir solution, which consisted of 100 mM sodium acetate pH 4.5, 400 mM sodium nitrate, and 30% ethylene glycol, was 250 μl per well. Lysozyme ($P1$) seeds were taken from storage at 243 K and diluted with reservoir buffer without ethylene glycol to 1:10,000, 1:20,000 and 1:40,000. The crystal was flash-cooled without additional cryoprotectant.

	Lysozyme ($P4_32_12$) ‡		**Lysozyme ($P1$)** §		
Experimental conditions	1st	2nd	1st	2nd	3rd
X-ray optics	Defining Φ100μm	Capillary focusing		Defining Φ100μm	
Beam size (μm)	Φ 100	Φ 80		Φ 100	
Wavelength (Å)	1.500			1.000	
Flux (Ph/sec)	3.23×10^{10}	5.80×10^{10}		3.92×10^{10}	
κ and φ (°)	0, 0	0, 0	0, 0	180, 0	180, 90
Oscillation angle (°)	0.1	0.1	0.1	0.1	0.1
Oscillation range (°)	90	90	360	360	360
Exp. time (sec)	0.2	0.1	0.1	0.1	0.1
Total exp. time (sec)	180	90	360	360	360
Detector distance (mm)	150			150	
Crystal size (μm^3)	50 × 50 × 100			100 × 100 × 100	
Statistics for XDS					
Space group	$P4_32_12$		$P1$		
Unit-cell parameters (Å, °)	a = 78.25, b = 78.25, c = 37.10, α, β, γ =90.00		a = 27.00, b =31.05, c =33.63, α = 88.09, β = 107.86, γ = 111.98		
Overall / inner / outer resolution shells (Å) *	50 – 1.75 / 50 – 5.21 / 1.86 – 1.75		50 – 1.12 / 50 – 3.34 / 1.19 – 1.12		
No. of images	900	900	3600	7200 (1st and 2nd)	10800 (1st, 2nd and 3rd)
Observed reflections †	72733 (2763, 11359)	72282 (2754, 11255)	117232 (4264, 17841)	233582 (8464, 36574)	349436 (12848, 54510)
Unique reflections †	22081 (841, 3556)	22080 (844, 3545)	65744 (2491, 10148)	72143 (2715, 11729)	73501 (2765, 12094)
Completeness †	99.4 (99.1, 99.3)	99.4 (99.2, 99.0)	88.9 (89.5, 85.6)	97.6 (97.2, 96.0)	99.4 (99.0, 99.0)
$\langle I/\delta(I)\rangle$ †	29.80 (49.34, 14.23)	35.01 (65.34, 14.00)	52.15 (85.61, 32.78)	55.31 (86.42, 35.80)	54.90 (83.75, 35.79)
R_{meas} (%)†	3.3 (2.4, 8.1)	2.7 (1.7, 8.5)	1.4 (1.4, 2.5)	1.7 (1.6, 2.8)	2.2 (2.0, 3.4)
CC(1/2) †	99.9 (99.9, 99.2)	99.9 (100.0, 99.2)	100.0 (99.9, 99.9)	100.0 (99.9, 99.9)	100.0 (99.9, 99.9)

APPARATUS FOR ACCURATE DIFFRACTION EXPERIMENTS

Crystal reorientation is sometimes required to improve the completeness of data for lower symmetry crystals, such as those belonging to space groups *P*1 and *C*2, and to resolve overlapping reflections from crystals of large unit cells. We developed a lightweight and compact κ and φ goniometer head, which was attached to a low eccentricity direct drive ω axis (Kohzu Precision). The κ and φ axes used high precision rotary positioners SR-2013 (SmarAct GmbH). The angle between the ω and κ axes was designed to be 15° (Figure 3(a)). The φ axis can open to 30° from the ω axis. The sample translation is performed on the X, Y, and Z axes installed in the ω axis. The ω axis can rotate ±270° with the κ and φ axes goniometer head. It referenced to various kinds of inverse-κ type goniometer [3, 10, 11].

Diffraction experiments were performed using hen egg-white lysozyme of space group *P*1 (lysozyme (*P*1)) crystals to confirm the performance of the goniometer head. Datasets were measured in the order of the ω axis only, the full open κ axis and the 90° rotation φ axis from the same crystal at wavelength of 1.0 Å (Table 1). The completeness of the data was improved by adding data from another crystal orientation.

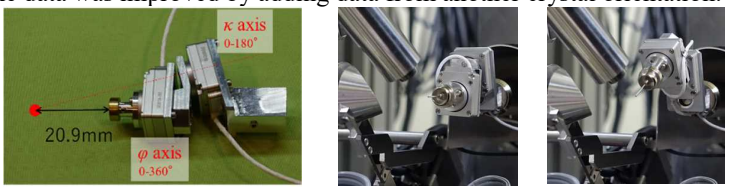

(a) (b) (c)

FIGURE 3. The κ and φ axes goniometer head attached to the ω axis. (a) The operating range of the κ and φ axes are 0 - 180° and 0 - 360°, respectively. The angle between the ω and κ axes is 15° (red dotted line). (b) View of the closed position of the κ axis. (c) View of the full open position of the κ axis.

SUMMARY

Upgraded beamline optics on DCM and additional focusing utilizing higher flux and higher density X-rays are described, and shown to reduce the X-ray irradiation time for high-efficiency data collection. In the future, this system will be introduced to the SPring-8 MX beamlines BL26B1 and B2, which have almost the same optics layout.

ACKNOWLEDGMENTS

This research was partially supported by Platform Project for Supporting Drug Discovery and Life Science Research (Basis for Supporting Innovative Drug Discovery and Life Science Research (BINDS)) from AMED under Grant Number JP18am0101070. This research was partially supported by RIKEN. All development and diffraction experiments were performed on the BL38B1 beamline at SPring-8 with the approval of the Japan Synchrotron Radiation Research Institute (JASRI; proposal nos. 2011B2084, 2014A1850, 2014A1899, 2014B1390, 2014B1965, 2014B1994, 2014B2004, 2014B2024, 2014B2029, 2015A1078, 2015A1994, 2015B1979, 2015B2078, 2016A1825, 2016A2515, 2016B1976, 2016B2515, 2017A1854, 2017A2562, 2017B2562, and 2018A2537).

REFERENCES

1. Goto, S. *et al.*, J. Synchrotron Rad. **5**, 1202–1205 (1998).
2. Yabashi, M. *et al.*, Proc. SPIE **3773**, 2–13 (1999).
3. Ueno, G. *et al.*, J. Struct. Funct. Genomics, **7**, 15-22 (2006).
4. Kawano, Y., *et al.*, In AIP Conf. Proc. **1234**, 359–362 (2010).
5. Baba, S., *et al.*, Acta Cryst. D **69,** 1839–1849 (2013).
6. Brauer, S., *et al.*, J. Synchrotron Rad. **2**, 163–173 (1995).
7. Fischetti, R. F., *et al.*, J. Synchrotron Rad. **16**, 217–225 (2009).
8. Gillilan, R. E., *et al.*, J. Synchrotron Rad. **17**, 227–236 (2010).
9. Kabsch, W., Acta Cryst. D **66**, 125–132 (2010).
10. Brockhauser, S., *et al.,* Acta Cryst. A **67**, 219–228 (2011).
11. Shi, W., *et al.,* J. Synchrotron Rad. **13**, 365-372 (2006).